Control Engineering Practice 19 (2011) 1363–1376

Contents lists available at ScienceDirect

Control Engineering Practice

journal homepage: www.elsevier.com/locate/conengprac

Steady-state drifting stabilization of RWD vehicles

Efstathios Velenis [a,*], Diomidis Katzourakis [b], Emilio Frazzoli [c], Panagiotis Tsiotras [d], Riender Happee [b]

[a] School of Engineering and Design, Brunel University, Uxbridge, Middlesex, UB8-3PH, UK
[b] Biomechanical Engineering Research Group (BMECHE), Technical University of Delft, 2628 CD Delft, The Netherlands
[c] Department of Aeronautics and Astronautics, Massachusetts Institute of Technology, Cambridge, MA 02139, USA
[d] Daniel Guggenheim School of Aerospace Engineering, Georgia Institute of Technology, Atlanta, GA 30332-0150, USA

ARTICLE INFO

Article history:
Received 20 July 2010
Accepted 12 July 2011
Available online 6 August 2011

Keywords:
Automotive control
Steady-states
Backstepping control
Vehicle dynamics
Limit handling

ABSTRACT

A control scheme to stabilize rear-wheel-drive (RWD) vehicles with respect to high-sideslip cornering (drifting) steady-states using coordinated steering and drive torque control inputs is presented in this paper. The choice of coordinated control inputs is motivated by the observed data collected during the execution of drifting maneuvers by an expert driver. In addition, the steering and drive torque input variables directly correlate to a human driver's steering wheel and throttle commands. The control design is based on a comprehensive vehicle model with realistic tire force and drive-train characteristics, and validated in a high-fidelity simulation environment.

1. Introduction

Recently, numerous studies on the dynamic behavior and control of vehicles have appeared in the literature, considering the vehicle's full handling capacity, e.g., with the tires operating in their nonlinear region. Researchers in the area of vehicle control and automotive safety envision that a new generation of active-safety systems for passenger vehicles will employ expert driving skills to actively assist the driver exploit the limits of handling of the vehicle during emergency manoeuvring, instead of restricting the vehicle's response within the linear region of operation of the tires.

A mathematical analysis of rally-race driving techniques, using nonlinear programming optimization, was initiated in Velenis and Tsiotras (2005), Velenis, Tsiotras, and Lu (2007a, 2007b), and Velenis, Tsiotras, and Lu (2008). These techniques clearly involve operation of the vehicle outside the stable operation envelope enforced by current active-safety systems, such as the electronic stability control (ESC) (van Zanten, Erhardt, Landesfeind, & Pfaff, 2000), as the vehicle reaches extreme sideslip angles and the tires operate in their nonlinear region. The analysis of rally driving techniques above reveals that minimum time and maximum exit speed cornering with limited preview of the road may require aggressive sideslip angles. In addition, the key role of longitudinal control (throttle/brake) and longitudinal weight transfer during cornering at high-sideslip angles was validated. In particular, expert rally drivers take advantage of weight transfer effects during acceleration and braking in order to change the under- or over-steering behavior of the vehicle.

The analysis in the above references provided a significant understanding of the dominant effects during the execution of expert driving techniques, but the open-loop numerical optimization approach does not compensate for uncertainties and disturbances encountered in real-life scenarios. Several studies have recently appeared in the literature, contributing to the closed-loop control formulation of the vehicle cornering problem at high sideslip angles as an equilibrium stabilization problem. Derivation of steady-state cornering equilibria with the tires operating in the nonlinear region, a stability analysis using phase-plane techniques, and the design of a robust stabilizing steering controller, under the assumption of complete absence of longitudinal forces (tractive or braking) at the tires, have appeared in Ono, Hosoe, Tuan, and Doi (1998). The analysis in Ono et al. (1998) was based on a low-order single-track model, which assumes equal forces at the tires of the same axle (front and rear). High-sideslip angle (drifting) steady-state cornering conditions were examined in Abdulrahim (2006) using the lateral dynamics, i.e., assuming fixed velocity, of a four-wheel rear-wheel-drive (RWD) vehicle model and a combined longitudinal/lateral tire friction model. The stability of steady-state drifting using a rich four-wheel RWD vehicle model, which incorporates longitudinal and lateral dynamics, weight transfer effects and a combined longitudinal/lateral tire friction model, has been discussed in Edelmann and Plöchl (2009). Derivation of drifting equilibria using vehicle models of lower order (and hence more appropriate for control design) has been discussed in Frazzoli (2008) and Hindiyeh and

* Corresponding author. Tel.: +44 1895 267589; fax: +44 1895 256392.
E-mail addresses: efstathios.velenis@brunel.ac.uk (E. Velenis), d.katzourakis@tudelft.nl (D. Katzourakis), frazzoli@mit.edu (E. Frazzoli), tsiotras@gatech.edu (P. Tsiotras), r.happee@tudelft.nl (R. Happee).

0967-0661/$ - see front matter © 2011 Elsevier Ltd. All rights reserved.
doi:10.1016/j.conengprac.2011.07.010

Gerdes (2009). In Frazzoli (2008) the author derived explicit steady-state cornering conditions for a single-track vehicle model using a combined longitudinal/lateral tire friction model, and considering longitudinal weight transfer effects. The simplifying assumption of a free rolling rear wheel in Frazzoli (2008), which suggests a front-wheel-drive (FWD) configuration, allowed for decoupling of the steady-state equations and efficient calculation of the equilibria. A stability analysis and classification of cornering equilibria, including drifting conditions, using a simple RWD single-track model with longitudinal and lateral dynamics and a simplified longitudinal/lateral tire friction model were presented in Hindiyeh and Gerdes (2009).

Stabilization of drifting equilibria appeared in Velenis, Frazzoli, and Tsiotras (2009), Velenis, Frazzoli, and Tsiotras (2010) and Voser, Hindiyeh, and Gerdes (2009), using low-order single-track vehicle models, and incorporating simplifying assumptions on the control inputs. In Velenis et al. (2009, 2010) a sliding mode control, using independent front- and rear-wheel drive/brake torque inputs, and assuming a fixed steering angle, was designed to stabilize the vehicle model with respect to drifting equilibria. In Voser et al. (2009) a steering controller considering only the lateral dynamics of a simple single-track model was designed to stabilize drifting equilibria, while a separate speed controller, considering the longitudinal vehicle dynamics only, was implemented to regulate the speed of the vehicle to the desired steady-state value. The control scheme in Voser et al. (2009) was implemented in an autonomous vehicle performing a drifting maneuver.

In this work, a control scheme, which stabilizes drifting equilibria of an RWD vehicle is presented, using coordinated lateral (steering) and longitudinal (drive torque) control inputs and mimicking techniques used by expert drivers. In contrast to previous works, simplifications associated with the use of solely longitudinal control (Velenis et al., 2009, 2010), solely lateral control (Ono et al., 1998), or decoupled longitudinal and lateral control (Voser et al., 2009), are avoided. Essentially, the controller proposed herein possesses the same control authority as a human driver. The coordinated longitudinal and lateral control, which corresponds to the operator's steering wheel and throttle commands, is motivated by the observation of data collected during the execution of drifting maneuvers by an expert race driver. Specifically, the data revealed that expert drivers use the throttle to induce high vehicle yaw rate and sideslip, that is, they use longitudinal inputs to control the lateral dynamics of the vehicle.

The control design is based on a comprehensive four-wheel vehicle model with realistic drive-train characteristics, instead of the simplified single-track model typically used in cornering stabilization applications. In order to overcome the complexity of the control design yielding from the high order vehicle model, the proposed control scheme consists of two layers: (a) Initially, a linear controller is designed to stabilize a reduced order system, derived by neglecting the wheel rotation dynamics. (b) The second layer of the control architecture employs a backstepping controller to regulate the wheel speed dynamics to their desired values from (a).

The next sections are organized as follows. Driver input and vehicle response data during the execution of steady-state drifting by an expert driver are presented first, and the driver steering, brake and throttle commands during the stabilization of the vehicle are analyzed. Next, the four-wheel vehicle model is introduced, incorporating nonlinear tire friction characteristics, longitudinal and lateral weight transfer effects, and coupling of the rear wheels drive torques through the modelling of a differential system. In the following section the steady-state tire friction forces and the associated drive torque and steering angle control inputs corresponding to drifting equilibria are computed numerically using the four-wheel vehicle model. Next, a linear controller is designed to stabilize the vehicle with respect to drifting equilibria using front-wheel steering angle and rear wheel rotation rates. A backstepping control scheme is also employed, providing the drive torque input necessary to regulate the rear-wheel speeds to the values dictated by the above linear controller. In the last sections, the control scheme is successfully validated in a high-fidelity simulation environment, and the conclusions of this work are summarized.

2. Experimental data of steady-state drifting

Data of driver control inputs and corresponding vehicle response collected during the execution of cornering maneuvers at high sideslip angles by an experienced rally driver are presented and analyzed in this section. These data will serve to support and validate the theoretical analysis later on in the paper. The data collection took place at the facilities of the Bill Gwynne Rally School in Brackley, UK, using a rally-race prepared 1980 Ford Escort with a 1.6 l engine producing approximately 110 bhp, and RWD transmission (Fig. 1).

2.1. Vehicle instrumentation

The vehicle vector velocity and sideslip angle were measured using a Racelogic VBox twin GPS antenna sensor. An inertial measurement unit (IMU) was placed on the centerline of the vehicle, behind the gear shifter, close to the estimated location of the vehicle's C.M., to measure 3-axis body accelerations and 3-axis body rotation rates. The rotational speed of each individual wheel was measured using externally fitted optical encoders. A string potentiometer was used to measure the steering angle at the steering column, and a rotational potentiometer was fitted on the throttle pedal to measure the pedal position. The vehicle was fitted with two brake pressure sensors to measure the brake pressure at the front and rear pairs of

Fig. 1. Vehicle and instrumentation used for data collection.

wheels. The handbrake, which is often used for vehicle control in rally driving, was integrated in the hydraulic brakes circuit and engaged the rear brakes only. Hence, the two brake sensors allowed us to distinguish between application of foot brake and handbrake, as well as to measure the brake balance between the front and rear wheels. The data were collected using a purpose-built data logger at 100 Hz. The vehicle instrumentation is described in detail in Katzourakis, Velenis, Abbink, Happee, and Holweg (to appear).

2.2. Test conditions and data analysis

The driver executed several drifting maneuvers on a loose surface (dirt), aiming at maintaining approximately constant speed and sideslip angle along a path of approximately constant radius. Two sets of data are analyzed, corresponding to two different steady-state conditions achieved by the driver, as shown in Fig. 2.

Data of the vehicle speed V, sideslip angle β, yaw rate $\dot{\psi}$ and individual wheel speeds ω_{ij}, $i=F$ (Front), R (Rear), $j=L$ (Left), R (Right), during the stabilization of the vehicle at a steady-state clockwise trajectory of radius approximately 13 m are shown in Fig. 4. The vehicle sideslip and yaw rate are positive along the counterclockwise direction. In the same figure the corresponding driver inputs are shown. Positive values of the steering angle of the front wheels δ correspond to turning left. The throttle pedal position is normalized by the value corresponding to the full throttle position. The front and rear axle brake pressures are normalized by the corresponding maximum value observed. The final part of the vehicle trajectory is shown in Fig. 2(a).

Throughout the 13 m radius trajectory the driver applied virtually no brake command, except from a small value along a brief interval around $t=21$ s. The vehicle started from a standstill and accelerated while cornering to the right. Between $5 \le t \le 10$ s the vehicle developed a high sideslip angle of approximately 30°. At the beginning of this interval full throttle was applied, resulting in the rear-wheels spinning at a considerably higher rate than the front ones. Consequently, the rear-wheel slip ratio, that is, the relative velocity of the rear tires with respect to the road along the longitudinal direction, was increased. The increased slip ratio resulted in the reduction of the cornering forces at the rear tires, in accordance to typical tire force characteristics during combined longitudinal/lateral tire motion (Fig. 3). The stabilizing yaw moment of the rear wheels was decreased with the decrease in the cornering forces, and the vehicle developed increased yaw rate and sideslip angle. The driver regulated the vehicle yaw moment by steering the front wheels towards the opposite direction with respect to the corner (counter-steered), while maintaining a high value of throttle input. For the unpowered front pair of wheels, the outer wheel with respect to the direction of the corner (front-left) rotated at a higher rate than the front inner (front-right) as it covered more distance during cornering. For the powered rear pair of wheels, the inner one rotated faster than the outer. This is due to the weight transfer away from the inner wheels during cornering, which resulted in lower friction forces, and hence less resistance to rotation under the application of drive torque. The vehicle was equipped with a limited slip differential (LSD) which prevented excessive differences in the rotation rates of the wheels at the rear axle. Peaks of sideslip angle at approximately $t=13$ and 17.5 s under high throttle and counter-steer commands can be observed in Fig. 4.

During the time interval $25 \le t \le 40$ s the vehicle speed was stabilized near 8.1 m/s, while the yaw rate fluctuated around an average value of 36°/s, which indeed corresponds to an approximate cornering radius of 13 m. The sideslip angle fluctuated around approximately 32°, and the driver applied throttle input close to

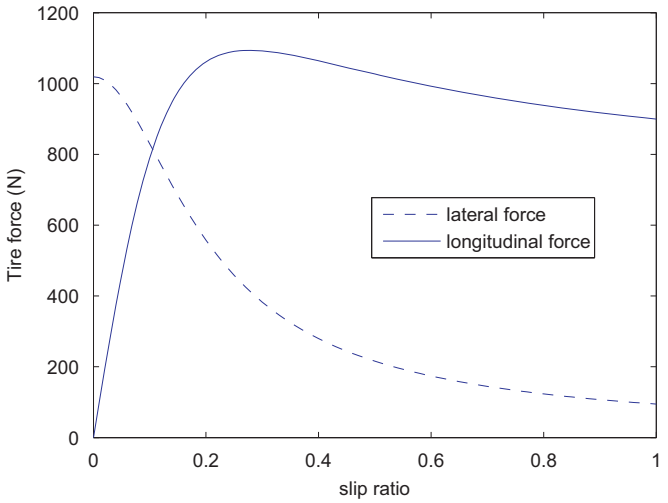

Fig. 3. Longitudinal and lateral tire forces for a range of slip ratio and a fixed value of tire slip angle computed using Pacejka's Magic Formula (Bakker, Nyborg, & Pacejka, 1987).

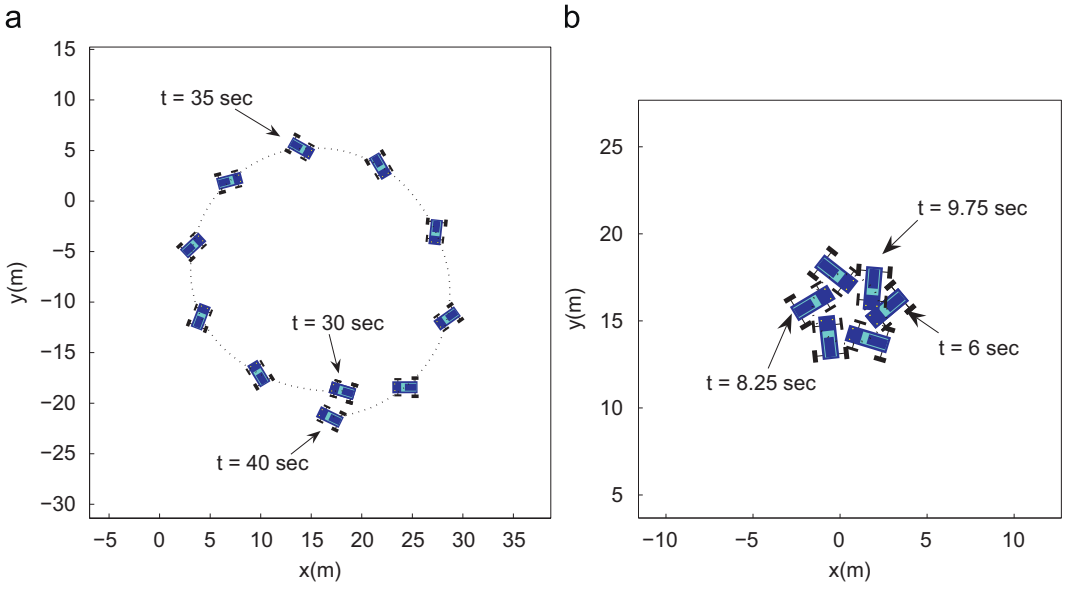

Fig. 2. Vehicle position and orientation data during steady-state cornering conditions of radius (a) 13 and (b) 2 m.

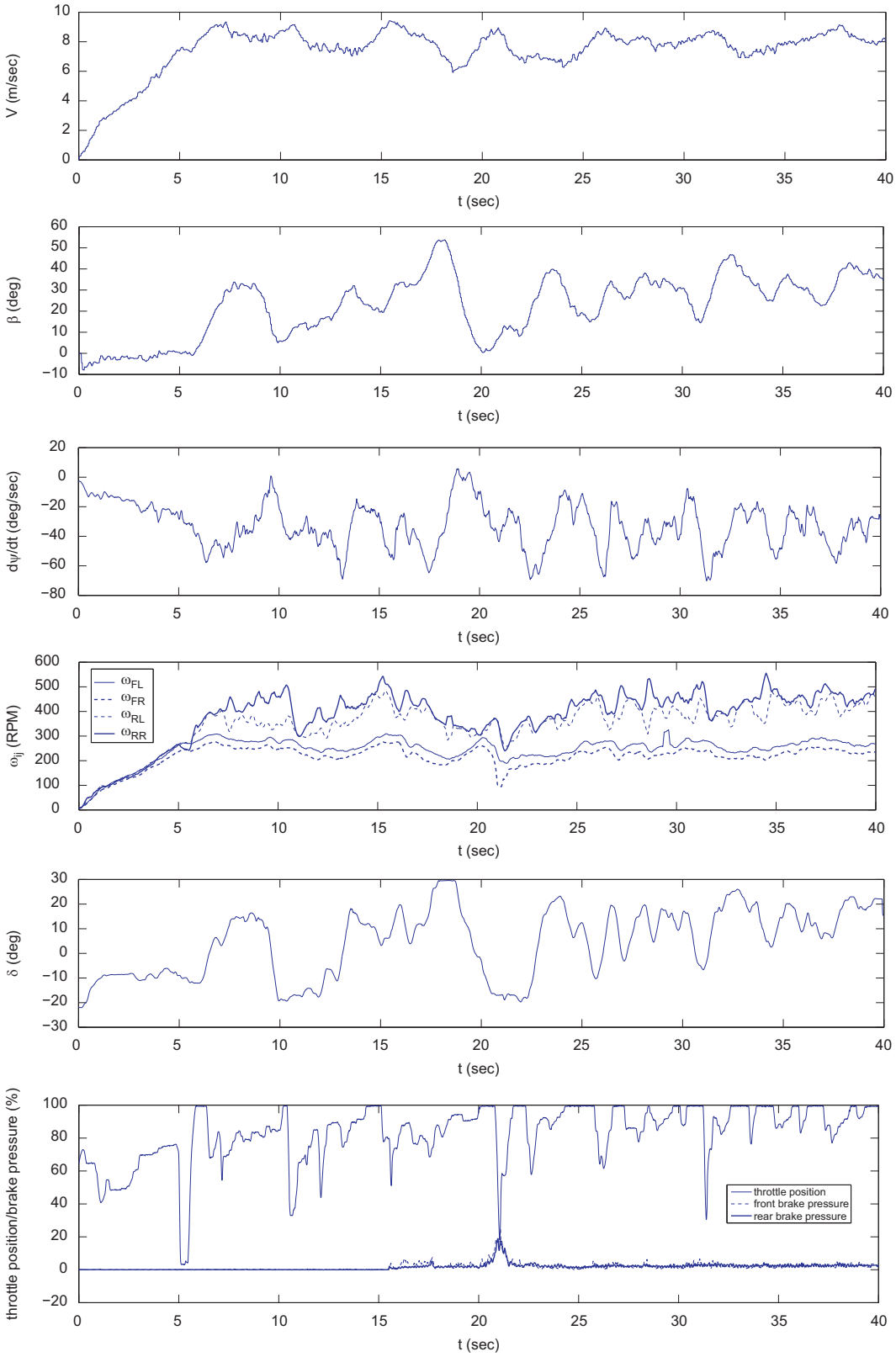

Fig. 4. Vehicle states and driver control inputs data along a steady-state trajectory of approximately 13 m of radius.

the maximum and consistently counter-steered. The corrections in the control inputs by the driver and the fluctuations of the vehicle states in this interval appear considerably smaller than in the previous interval $t \leq 25$ s, and hence one may conclude that the driver was attempting to stabilize the vehicle states to the above average values. Cornering at high sideslip angles with the rear wheels slipping under high drive torque (in RWD vehicles) is also referred to, in the racing community, as power-oversteer or powerslide. The powerslide is an unstable driving condition (Edelmann & Plöchl, 2009), hence the driver's intervention is required for external disturbances to be attenuated. The uneven rough surface of the rally course offers a disturbance rich environment (e.g., bumps and dips in

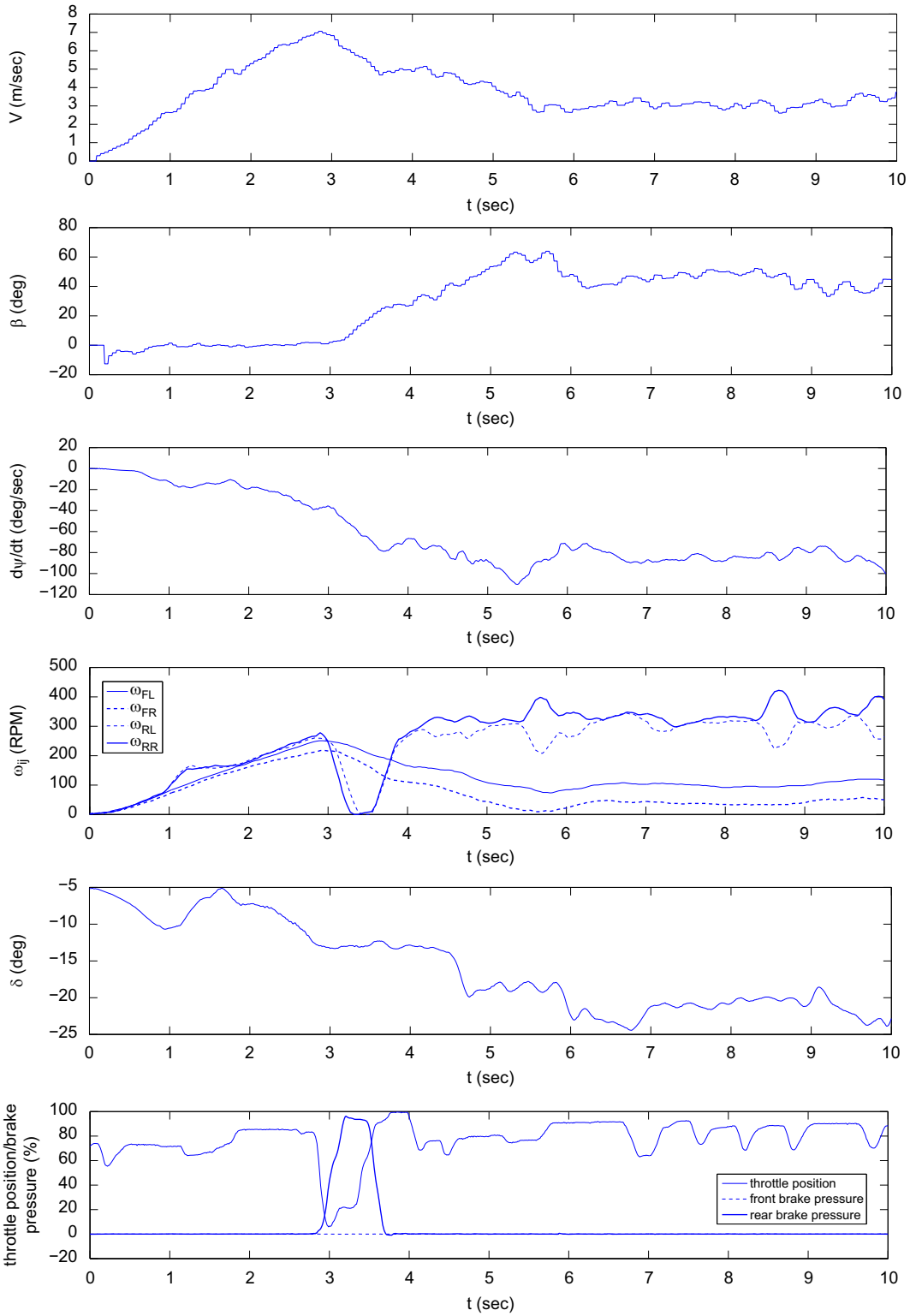

Fig. 5. Vehicle states and driver control inputs data along a steady-state trajectory of approximately 2 m of radius.

the testing area affecting the vertical axis equilibrium and/or variations in the friction coefficient) for the stabilization task, which explains the fluctuations in the vehicle states and driver's control inputs.

Fig. 5 shows the vehicle states and driver control inputs during the stabilization of the vehicle at a steady-state clockwise trajectory of approximately 2 m of radius. The final part of the trajectory is shown in Fig. 2(b). The vehicle started from a standstill and accelerated while cornering to the right. In the interval $0 \leq t \leq 3$ s the velocity and yaw rate increased smoothly at a low sideslip angle. At approximately $t=3$ s the driver applied a handbrake command as indicated by the increase in the rear brake pressure, with the front brake pressure remaining at zero. The speed of the rear wheels dropped to zero (wheel lock), which corresponds to an increase in the magnitude of the slip ratio, and consequently a decrease in the rear wheels lateral forces. As a result the vehicle yaw rate and sideslip angle increased in

magnitude. The driver was then back on the throttle, releasing the handbrake and maintaining a high rate of rotation of the rear wheels. In the interval $6 \le t \le 10$ s the vehicle was stabilized to a velocity of approximately 3 m/s, a yaw rate of 1.5 rad/s (indicating a steady-state path radius of 2 m), and a sideslip angle of 45°. It is worth noting that, as in the previous steady-state condition, during the steady-state cornering interval the driver maintained a throttle command close to the maximum. However, in this case the steering angle was consistently towards the direction of the corner, as opposed to the counter-steering observed in the previous set of data. This is in contrast to definitions of drifting or powerslide in Edelmann and Plöchl (2009), Hindiyeh and Gerdes (2009), and Voser et al. (2009), where counter-steering is considered as an essential characteristic. The above references, however, did not consider small cornering radii. In addition, it is noted that the vehicle states and driver control inputs demonstrate considerably smaller fluctuations around their average values compared to the 13 m trajectory. The 2 m maneuver took place within a limited area in the testing grounds (Fig. 2(b)), with considerably reduced probability of a disturbance occurrence. Finally, it is worth highlighting that with such a drifting maneuver the driver expanded the mobility capabilities of the vehicle achieving a cornering radius which is considerably less than its kinematic characteristics dictate. Assuming no wheel slip, the minimum kinematic cornering radius depends on the maximum allowable steering angle, and increases proportionally to the wheelbase (distance between front and rear axles) (Gillespie, 1992). The minimum kinematic cornering radius of the test vehicle was 4.5 m.

3. Vehicle model

A four-wheel vehicle model is introduced in this section for the derivation of the steady-state drifting conditions and the design of a stabilizing controller. Nonlinear tire force characteristics with coupled longitudinal and lateral components, as well as the effects of weight transfer between the four wheels arising from the longitudinal and lateral acceleration of the vehicle, are incorporated. By modelling the operation of a limited slip differential, the drive torques of the left and right wheels of the driven axle are coupled to a single torque control input, which correlates directly to the driver's throttle command.

3.1. Equations of motion

The equations of motion of a four-wheel vehicle, with front-wheel steering, travelling on a horizontal plane (Fig. 6) are given as follows:

$$m\dot{V} = (f_{FLx}+f_{FRx})\cos(\delta-\beta)-(f_{FLy}+f_{FRy})\sin(\delta-\beta) + (f_{RLx}+f_{RRx})\cos\beta+(f_{RLy}+f_{RRy})\sin\beta, \quad (1)$$

$$\dot{\beta} = \frac{1}{mV}[(f_{FLx}+f_{FRx})\sin(\delta-\beta)+(f_{FLy}+f_{FRy})\cos(\delta-\beta) -(f_{RLx}+f_{RRx})\sin\beta+(f_{RLy}+f_{RRy})\cos\beta]-\dot{\psi}, \quad (2)$$

$$I_z\ddot{\psi} = \ell_F[(f_{FLy}+f_{FRy})\cos\delta+(f_{FLx}+f_{FRx})\sin\delta] -\ell_R(f_{RLy}+f_{RRy})+w_L(f_{FLy}\sin\delta-f_{FLx}\cos\delta-f_{RLx}) +w_R(f_{FRx}\cos\delta-f_{FRy}\sin\delta+f_{RRx}), \quad (3)$$

$$I_w\dot{\omega}_{ij} = T_{ij}-f_{ijx}r, \quad i=F,R,\ j=L,R. \quad (4)$$

In the above equations m is the vehicle's mass, I_z is the moment of inertia of the vehicle about the vertical axis, V is the vehicle velocity at the center of mass (C.M.), β is the sideslip angle at the C.M. and ψ is the yaw angle. The moment of inertia of each wheel about its axis of rotation is I_w, the radius of each wheel is r, and the rotation rate of each wheel is ω_{ij} ($i=F,R$, $j=L,R$). The steering angle of the front wheels (assuming equal angle for left and right front wheels) is denoted by δ, and the drive/brake torque applied on each wheel is T_{ij}.

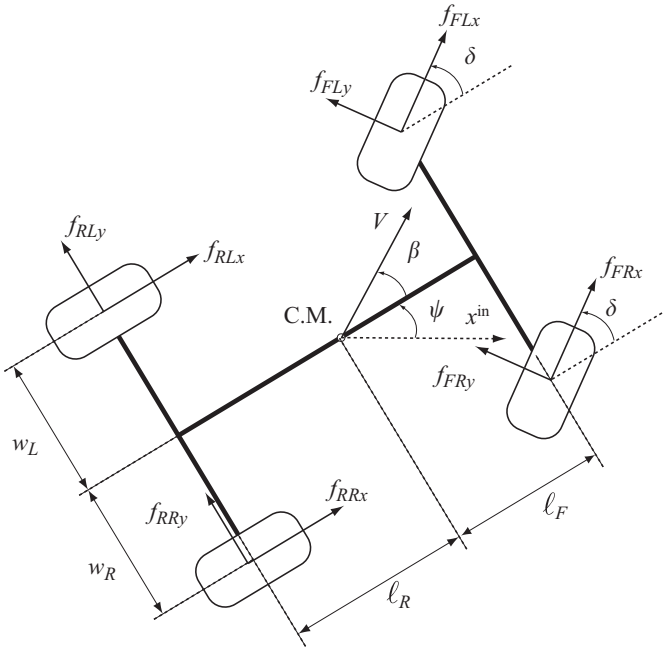

Fig. 6. Full-car vehicle model travelling on a horizontal plane. The inertial frame x-axis is denoted by x^{in}.

The rolling resistances and self-aligning moments at the tires have been neglected. The longitudinal and lateral friction forces at each wheel are denoted by f_{ijk} ($i=F,R$, $j=L,R$ and $k=x,y$). The distances ℓ_F, ℓ_R, w_L and w_R determine the location of the C.M. with respect to the center of each wheel, as in Fig. 6.

3.2. Tire forces

The tire forces f_{ijk} in the above vehicle model are calculated as functions of tire slip using Pacejka's Magic Formula (MF) (Bakker, Nyborg, & Pacejka, 1987). Tire slip refers to the non-dimensional relative velocity of the tire with respect to the road. In Bakker et al. (1987) the practical tire slip quantities, namely the practical longitudinal slip κ_{ij} and the slip angle α_{ij}, are defined as follows:

$$\kappa_{ij} = \frac{\omega_{ij}r_{ij}-V_{ijx}}{V_{ijx}}, \quad \tan\alpha_{ij} = \frac{V_{ijy}}{V_{ijx}}, \quad i=F,R,\ j=L,R,$$

where V_{ijk} ($i=F,R$, $j=L,R$, $k=x,y$) are the tire frame components of the vehicle velocity vector at the centers of the four wheels.

The theoretical slip quantities (Bakker et al., 1987) are defined as:

$$s_{ijx} = \frac{V_{ijx}-\omega_{ij}r_{ij}}{\omega_{ij}r_{ij}} = -\frac{\kappa_{ij}}{1+\kappa_{ij}}, \quad (5)$$

$$s_{ijy} = \frac{V_{ijy}}{\omega_{ij}r_{ij}} = \frac{\tan\alpha_{ij}}{1+\kappa_{ij}} = (1+s_{ijx})\frac{V_{ijy}}{V_{ijx}}. \quad (6)$$

The resultant slip at each tire is defined by

$$s_{ij} = \sqrt{s_{ijx}^2+s_{ijy}^2}. \quad (7)$$

Assuming linear dependence of the tire friction forces on the tire vertical force one obtains

$$\mu_{ij} = f_{ij}/f_{ijz}, \quad \mu_{ijk} = f_{ijk}/f_{ijz}, \quad i=F,R,\ j=L,R,\ k=x,y, \quad (8)$$

where $f_{ij} = \sqrt{f_{ijx}^2+f_{ijy}^2}$ is the resultant friction force on the plane of the road surface, μ_{ij} is the resultant friction coefficient, μ_{ijk} are the longitudinal and lateral friction coefficients, and f_{ijz} are the vertical forces at each of the four wheels.

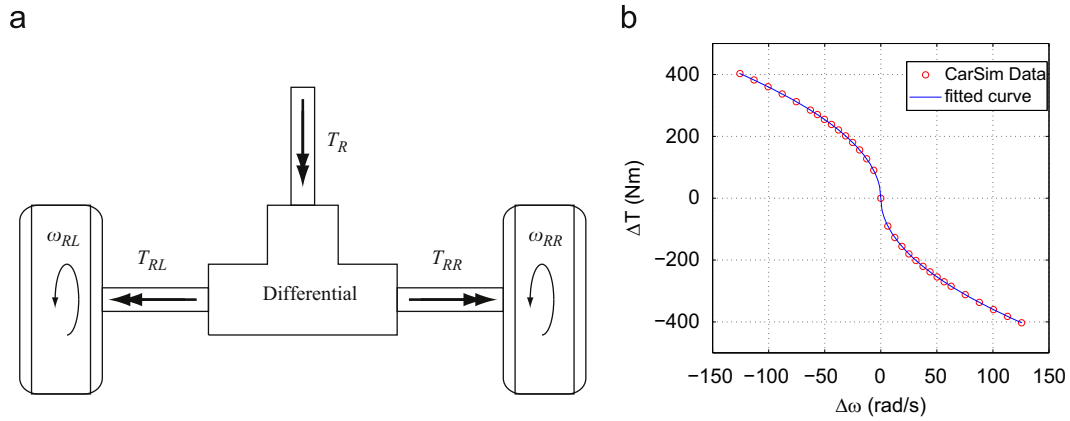

Fig. 7. (a) Operation of a differential system and (b) LSD torque transfer characteristic.

The resultant friction coefficient is calculated using the simplified Pacejka's MF (Bakker et al., 1987) as follows:

$$\mu_{ij}(s_{ij}) = \mathrm{MF}(s_{ij}) = D\sin(C\mathrm{atan}(Bs_{ij})). \tag{9}$$

Assuming symmetric tire characteristics with respect to the longitudinal and lateral directions, the total friction force for each tire lies within the so-called friction circle. In this case, the longitudinal and lateral tire friction components are given by:

$$\mu_{ijk} = -\frac{s_{ijk}}{s_{ij}}\mu_{ij}(s_{ij}). \tag{10}$$

Finally, neglecting the vertical motion and pitch and roll rotations of the sprung mass of the vehicle, the vertical force at each of the four wheels is calculated by considering the static weight distribution and longitudinal/lateral weight transfer under longitudinal/lateral acceleration. The total vertical force at each wheel is given by:

$$f_{FLz} = f^0_{FLz} - \Delta f^x_L - \Delta f^y_F, \quad f_{FRz} = f^0_{FRz} - \Delta f^x_R + \Delta f^y_F,$$

$$f_{RLz} = f^0_{RLz} + \Delta f^x_L - \Delta f^y_R, \quad f_{RRz} = f^0_{RRz} + \Delta f^x_R + \Delta f^y_R. \tag{11}$$

Under conditions of zero longitudinal and lateral acceleration of the vehicle, the static vertical force distribution results in:

$$f^0_{FLz} = \frac{mg\ell_R w_R}{(\ell_F+\ell_R)(w_L+w_R)}, \quad f^0_{FRz} = \frac{mg\ell_R w_L}{(\ell_F+\ell_R)(w_L+w_R)},$$

$$f^0_{RLz} = \frac{mg\ell_F w_R}{(\ell_F+\ell_R)(w_L+w_R)}, \quad f^0_{RRz} = \frac{mg\ell_F w_L}{(\ell_F+\ell_R)(w_L+w_R)}. \tag{12}$$

Neglecting the roll motion of the sprung mass, acceleration a_y along the lateral body axis results in weight transfer from front-left to front-right and rear-left to rear-right wheels as follows (Gillespie, 1992):

$$\Delta f^y_F = \frac{mh\ell_R}{(\ell_F+\ell_R)(w_L+w_R)}a_y, \quad \Delta f^y_R = \frac{mh\ell_F}{(\ell_F+\ell_R)(w_L+w_R)}a_y, \tag{13}$$

where h is the distance of the vehicle's C.M. from the road level. Similarly, acceleration a_x along the longitudinal body axis results in weight transfer from front-left to rear-left and from front-right to rear-right wheels as follows:

$$\Delta f^x_L = \frac{mhw_R}{(\ell_F+\ell_R)(w_L+w_R)}a_x, \quad \Delta f^x_R = \frac{mhw_L}{(\ell_F+\ell_R)(w_L+w_R)}a_x. \tag{14}$$

3.3. Modelling of the rear axle differential system

The model of a limited slip differential (LSD) system, which provides coupling of the drive torques of the driven rear-left and rear-right wheels, is introduced in this section. The differential is the device of the drive-train of the vehicle that distributes the torque from the engine/gearbox assembly to the wheels of the driven axle (Fig. 7(a)). Considering a RWD vehicle and assuming no braking command, the front wheel torques become $T_{Fj} = 0$, $(j = L,R)$. The output drive torque T_R from the gearbox will then be distributed between the rear-left and rear-right wheels, providing T_{RL} and T_{RR} in Eq. (4). An LSD system transfers torque from the wheel that is spinning faster to the slower spinning wheel. The aim of the LSD is to transfer torque to the wheel that provides higher traction, and limit slipping of the wheel with lower traction.

The torque transfer characteristics of an LSD differential model of the CarSim vehicle simulation software (CarSim, 2009) was used in this work. The torque transfer as a function of the wheel speed differential is provided in CarSim in the form of a look-up table. The data of the look-up table were used to identify an explicit expression of the differential torque transfer as a function of the wheel speed differential. The following formula is fitted to the CarSim data, as shown in Fig. 7(b):

$$\Delta T(\Delta\omega) = -\mathrm{sign}(\Delta\omega)C_d\sqrt{|\Delta\omega|}, \tag{15}$$

where $\Delta T = T_{RL} - T_{RR}$, $\Delta\omega = \omega_{RL} - \omega_{RR}$, and C_d is a positive constant.

By introducing the single torque input $T_R = T_{RL} + T_{RR}$, corresponding to the torque applied from the gearbox to the differential system input shaft, the rear-left and rear-right wheel torques are given as follows:

$$T_{RR} = \frac{T_R - \Delta T(\Delta\omega)}{2}, \quad T_{RL} = \frac{T_R + \Delta T(\Delta\omega)}{2}, \tag{16}$$

where $\Delta T(\Delta\omega)$ from (15). Finally, using Eqs. (4), (15) the dynamics of the rear wheels speed differential are derived as follows:

$$I_w\frac{\mathrm{d}\Delta\omega}{\mathrm{d}t} = \Delta T(\Delta\omega) - (f_{RLx} - f_{RRx})r. \tag{17}$$

4. Steady-state cornering conditions

Steady-state cornering is characterized by a trajectory of constant radius $R = R^{ss}$, negotiated at a constant speed $V = V^{ss}$, constant yaw rate $\dot\psi = \dot\psi^{ss} = V^{ss}/R^{ss}$, constant sideslip angle $\beta = \beta^{ss}$, and constant wheel speeds $\omega_{ij} = \omega^{ss}_{ij}$. During steady-state cornering, the control inputs, namely the steering angle $\delta = \delta^{ss}$ and rear axle torque $T_R = T^{ss}_R$, also remain constant.

Enforcing the steady-state cornering conditions

$$\dot V = 0, \quad \dot\beta = 0, \quad \ddot\psi = 0, \quad \dot\omega_{ij} = 0, \tag{18}$$

and considering an RWD transmission and no braking command, that is, enforcing free rolling of the front wheels

$$s^{ss}_{Fjx} = 0, \quad f^{ss}_{Fjx} = 0, \quad T^{ss}_{Fj} = 0, \quad j = L,R, \tag{19}$$

and providing fixed values for the steady-state pair (R^{ss},β^{ss}), one is able to solve numerically the set of nonlinear algebraic equations (1)–(16) for the rest of the steady-state variables V^{ss}, ω_{ij}^{ss}, steady-state slip quantities and tire forces s_{ijk}^{ss}, f_{ijk}^{ss}, vertical forces at the wheels f_{ijz}^{ss}, and steady-state control inputs δ^{ss} and T_R^{ss} ($i=F,R$, $j=L,R$, $k=x,y$). Fixing the values for (R^{ss},β^{ss}) results in a number of unknown parameters equal to the number of Eqs. (1)–(16). Alternatively, one may provide fixed values for different parameters, for instance (R^{ss},V^{ss}), or (V^{ss},β^{ss}), and solve for the remaining state and control variables. In this work the nonlinear equation solver of Matlab was employed. A similar derivation, using a single-track model, is presented in more detail in Velenis et al. (2010).

Clockwise cornering equilibria for a range of path radii R^{ss} and sideslip angles β^{ss}, using the vehicle and tire model parameters of Table 1, are given in Fig. 8. In particular, the steady-state value of the centripetal acceleration $a_{cent}^{ss}=(V^{ss})^2/R^{ss}$ for each steady-state pair (R^{ss},β^{ss}) is shown. The solid line passes through the points of maximum a_{cent}^{ss} considering fixed values of R^{ss}. The existence of steady-state conditions at extremely low path radii ($R^{ss}<4.5$ m) may expand the mobility characteristics of the vehicle. Along paths of low radii the vehicle achieves the highest speed equilibria at higher sideslip angles. In Fig. 9 the steady-state conditions corresponding to $R^{ss}=13$ and 2 m are shown. The maximum steady-state centripetal acceleration, and hence the maximum steady-state speed, is achieved at approximately 30° of sideslip angle along the 13 m radius path, whereas in the case of the 2 m path radius the maximum speed is achieved at a more aggressive sideslip angle of 55°. In the case of $R^{ss}=13$ m the steady-state steering command corresponds to counter-steering ($\delta>0$ along a right turn) for increased values of sideslip ($\beta^{ss}>25°$). In the case of $R^{ss}=2$ m the steering command is along the direction of corner for sideslip angle up to 55°, and countersteering is required for higher values of sideslip. A cornering equilibrium along $R^{ss}=2$ m with a less aggressive sideslip angle $\beta^{ss}<30°$ would require a high value of steering angle $|\delta|>35°$ which may exceed the limits of the steering system, hence driving along extremely low radii becomes practically possible only with drifting.

Table 1
Estimated test-vehicle parameters.

Parameter	Value	Parameter	Value
m (kg)	850	ℓ_F (m)	1.5
I_z (kg m^2)	1400	ℓ_R (m)	0.9
I_w (kg m^2)	0.6	r (m)	0.311
w_L,w_R (m)	0.74	B	4
C_d Nm/(rad/s)$^{1/2}$	50	C	1.3
h (m)	0.5	D	0.6

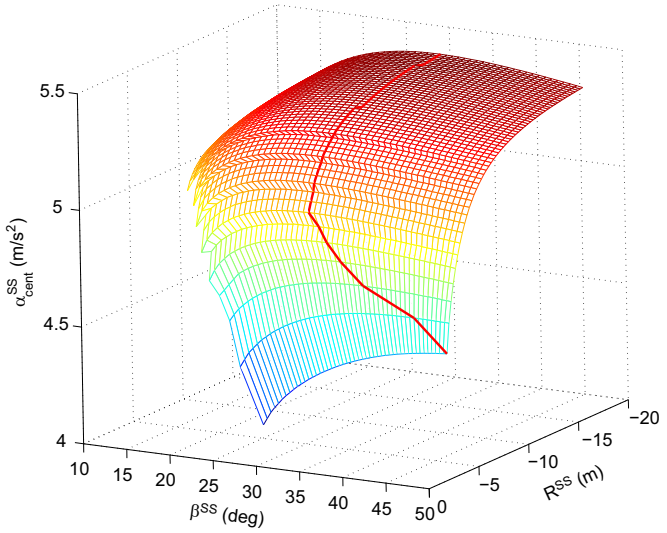

Fig. 8. Calculated steady-state equilibria.

In Table 2 the steady-state conditions achieved during the data collection experiment of Section 2 are compared to the calculated steady-state conditions using the four-wheel vehicle model of Table 1. Despite the uncertainty in many of the vehicle and tire parameters, the calculated steady-states closely match the data.

As shown in Edelmann and Plöchl (2009), drifting equilibria are unstable, which can also be verified through linearization of the system dynamics (1)–(4) with respect to the equilibrium states, assuming control inputs fixed at their steady-state values, and calculation of the eigenvalues of the Jacobian Matrix. The linearized input–output system, which is discussed in the next section, can also be used to study the controllability and stabilizability of each equilibrium. The controllability matrix was computed for all equilibrium points of Fig. 8 and found to be of full rank, revealing that all the equilibria calculated are controllable. While the above does not provide proof of controllability of all the existing steady-states, as the calculation was performed for a fixed set of vehicle parameters and only a subset of all possible equilibria, the determination of the stabilizability of the steady-states is necessary, before one can proceed with the control design.

5. Stabilization of steady-state cornering

A control scheme to stabilize an RWD vehicle with respect to drifting equilibria, using control inputs directly correlating to driver commands, is presented next. The proposed architecture consists of a linear controller providing stabilizing front-wheel steering angle (corresponding to the driver's steering command), and rear-wheel angular rate inputs. In addition, a backstepping controller calculates the rear differential drive torque necessary for the rear-left and rear-right wheels to achieve the wheel speeds dictated by the previous linear controller.

5.1. Steering and rear-wheel speed control

Neglecting the dynamics of each individual wheel rotation (Eq. (4)), the equations of motion of the full-car model (1)–(3), including the rear-wheel speed differential equation (17), are expressed as a system driven by the steering angle control input $\hat{\delta}$ and one of the rear-wheel angular rates, for instance the rear-left wheel rotational speed input $\hat{\omega}_{RL}$:

$$\frac{d}{dt}V=f_1(V,\beta,\dot{\psi},\Delta\omega,\hat{\omega}_{RL},\hat{\delta}), \tag{20}$$

$$\frac{d}{dt}\beta=f_2(V,\beta,\dot{\psi},\Delta\omega,\hat{\omega}_{RL},\hat{\delta}), \tag{21}$$

$$\frac{d}{dt}\dot{\psi}=f_3(V,\beta,\dot{\psi},\Delta\omega,\hat{\omega}_{RL},\hat{\delta}), \tag{22}$$

$$\frac{d}{dt}\Delta\omega=f_4(V,\beta,\dot{\psi},\Delta\omega,\hat{\omega}_{RL}). \tag{23}$$

The rear-right wheel speed ω_{RR} is calculated using the state variable $\Delta\omega$ and the rear-left wheel speed input $\hat{\omega}_{RL}$. Hence, one may calculate longitudinal and lateral friction forces at both rear wheels, using the tire model of Section 3.2. Free rolling of the front wheels is also enforced (see (19)).

The equilibrium states $(V^{ss},\beta^{ss},\dot{\psi}^{ss},\Delta\omega^{ss})$ and inputs $(\omega_{RL}^{ss},\delta^{ss})$ are calculated as in Section 4. Eqs. (20)–(23) are linearized as follows:

$$\frac{d\mathbf{x}}{dt}=\mathcal{A}^{ss}\mathbf{x}+\mathcal{B}^{ss}\mathbf{u}=\mathcal{A}^{ss}\mathbf{x}+\mathcal{B}_1(\hat{\omega}_{RL}-\omega_{RL}^{ss})+\mathcal{B}_2(\hat{\delta}-\delta^{ss}),$$

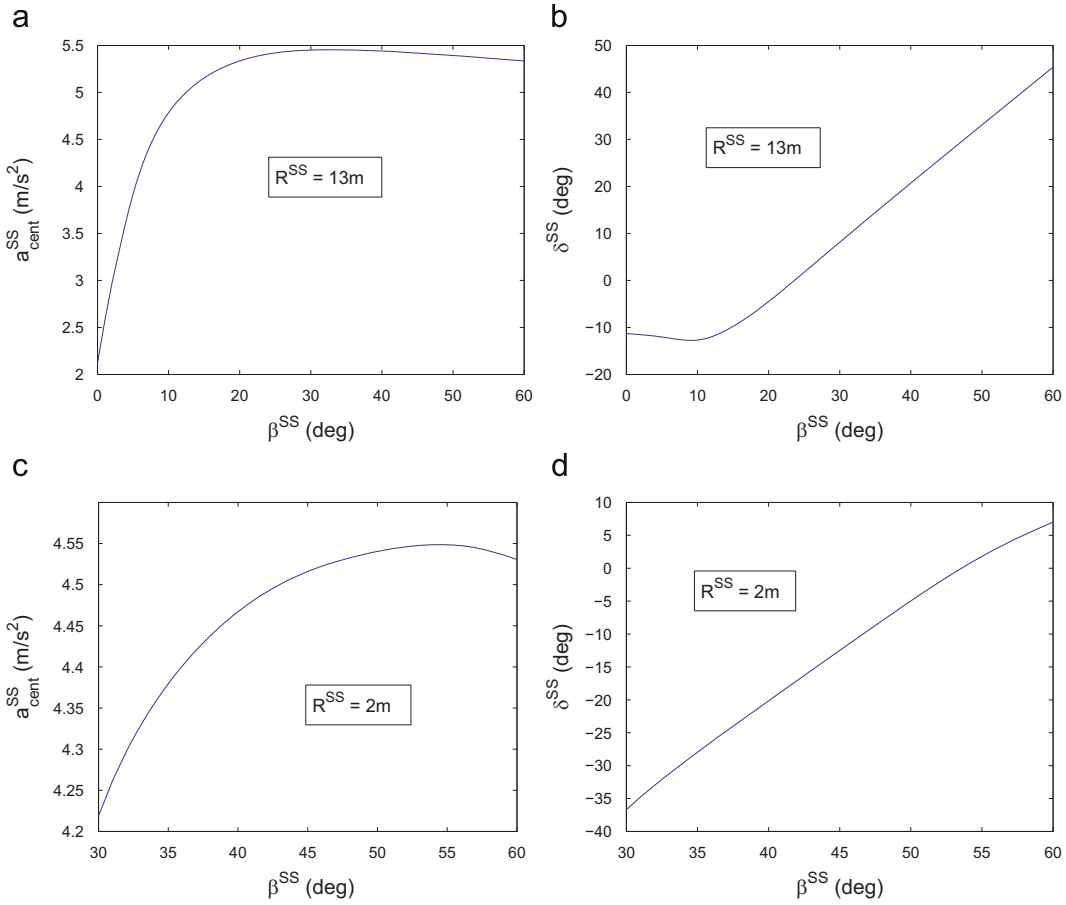

Fig. 9. Steady-state cornering equilibria for fixed values of R^{ss} and a range of β^{ss}.

Table 2
Steady-state drifting condition.

Variable	Data	Calculated	Data	Calculated
R^{ss} (m)	13	13	2	2
V^{ss} (m/s)	8.1	8.42	3.1	3
β^{ss} (deg.)	31.4	33	44	40
$\dot{\psi}^{ss}$ (deg./s)	−35.7	−37.1	−88.8	−85.6
ω_{FL}^{ss} (RPM)	265.3	249.5	102.2	101.3
ω_{FR}^{ss} (RPM)	230.9	220.7	41.3	37.5
ω_{RL}^{ss} (RPM)	409	347.2	302.8	223.5
ω_{RR}^{ss} (RPM)	451.7	393.5	341.4	272.7
δ^{ss} (deg.)	12.5	11.9	−21.6	−20.1

$$\mathbf{y} = \mathcal{C}\mathbf{x}, \tag{24}$$

where $\mathcal{A}^{ss}$ and $\mathcal{B}^{ss}$ are the Jacobian matrices, computed at the equilibrium point, $\mathbf{B_1}$ and $\mathbf{B_2}$ are the first and second columns of $\mathbf{B}^{ss}$, respectively, and

$$\mathbf{x} = \begin{bmatrix} V - V^{ss} \\ \beta - \beta^{ss} \\ \dot{\psi} - \dot{\psi}^{ss} \\ \Delta\omega - \Delta\omega^{ss} \end{bmatrix}, \quad \mathbf{u} = \begin{bmatrix} \hat{\omega}_{RL} - \omega_{RL}^{ss} \\ \hat{\delta} - \delta^{ss} \end{bmatrix}, \quad \mathcal{C} = \mathcal{I}^{4\times 4}.$$

The control

$$\mathbf{u} = -\mathbf{K}\mathbf{x}, \tag{25}$$

where the control gain matrix $\mathbf{K}$ is given by

$$\mathbf{K} = \mathbf{R}^{-1}(\mathbf{B}^{ss})^T\mathbf{P}$$

and $\mathbf{P}$ is the symmetric positive-definite solution to the following algebraic Riccati equation:

$$(\mathbf{A}^{ss})^T\mathbf{P} + \mathbf{P}\mathbf{A}^{ss} - \mathbf{P}\mathbf{B}^{ss}\mathbf{R}^{-1}(\mathbf{B}^{ss})^T\mathbf{P} + \mathbf{C}^T\mathbf{Q}\mathbf{C} = \mathbf{0}, \tag{26}$$

stabilizes the equilibrium $\mathbf{x}=\mathbf{0}$ and minimizes the quadratic cost

$$\mathbf{J} = \int_0^\infty [\mathbf{y}(t)^T\mathbf{Q}\mathbf{y}(t) + \mathbf{u}(t)^T\mathbf{R}\mathbf{u}(t)]\,\mathrm{d}t.$$

The matrix $\mathbf{Q}$ is real, symmetric and positive semi-definite, and matrix $\mathbf{R}$ is real, symmetric and positive definite.

Letting $\mathbf{K_1}$ and $\mathbf{K_2}$ be the first and second rows of the gain matrix $\mathbf{K}$, respectively, the linear quadratic regulator (25) provides the following rear-wheel angular rate and steering angle commands:

$$\hat{\omega}_{RL}(\mathbf{x}) = -\mathbf{K_1}\mathbf{x} + \omega_{RL}^{ss}, \tag{27}$$

$$\hat{\delta}(\mathbf{x}) = -\mathbf{K_2}\mathbf{x} + \delta^{ss}. \tag{28}$$

5.2. Drive torque control

Next, a backstepping controller (Kokotovic, 1992) is designed using the rear drive torque T_R to regulate the rotational speeds of the rear wheels to the values generated by the control law (25).

The variable z_{RL} is defined as the difference between the actual wheel angular rate ω_{RL} and the reference value $\hat{\omega}_{RL}(\mathbf{x})$:

$$z_{RL} = \omega_{RL} - \hat{\omega}_{RL}(\mathbf{x}). \tag{29}$$

Eqs. (4) and (29) result in

$$\dot{z}_{RL} = \dot{\omega}_{RL} - \frac{\partial\hat{\omega}_{RL}(\mathbf{x})}{\partial\mathbf{x}}\dot{\mathbf{x}} = \frac{1}{I_w}T_{RL} - \frac{r}{I_w}f_{RLx} + \mathbf{K_1}[\dot{V}\;\dot{\beta}\;\ddot{\psi}\;\Delta\dot{\omega}]^T. \tag{30}$$

Taking

$$T_{RL} = f_{RLx} r - I_w \mathbf{K_1} [f_1 \ f_2 \ f_3 \ f_4]^T + I_w v, \tag{31}$$

and applying the steering controller (28), the linearized equations (24) are now extended to incorporate the wheel speed error dynamics $\dot{z}_{RL}$ as follows:

$$\begin{aligned}\dot{\mathbf{x}} &= \mathbf{A}^{ss}\mathbf{x} + \mathbf{B_1}(\omega_{RL} - \omega_{RL}^{ss}) + \mathbf{B_2}(\hat{\delta}(\mathbf{x}) - \delta^{ss}) \\ &= \mathbf{A}^{ss}\mathbf{x} + \mathbf{B_1}(z_{RL} + \hat{\omega}_{RL}(\mathbf{x}) - \omega_{RL}^{ss}) + \mathbf{B_2}(\hat{\delta}(\mathbf{x}) - \delta^{ss}) \\ &= (\mathbf{A}^{ss} - \mathbf{B}^{ss}\mathbf{K})\mathbf{x} + \mathbf{B_1} z_{RL},\end{aligned}$$

$$\dot{z}_{RL} = v. \tag{32}$$

The Lyapunov function candidate

$$\mathcal{V}(\mathbf{x}, z_{RL}) = \mathbf{x}^T \mathbf{P} \mathbf{x} + \tfrac{1}{2} z_{RL}^2, \tag{33}$$

where $\mathbf{P}$ is given by (26), yields

$$\begin{aligned}\dot{\mathcal{V}} &= \mathbf{x}^T[(\mathbf{A}^{ss} + \mathbf{B}^{ss}\mathbf{K})^T\mathbf{P} + \mathbf{P}(\mathbf{A}^{ss} + \mathbf{B}^{ss}\mathbf{K})]\mathbf{x} + 2\mathbf{x}^T\mathbf{P}\mathbf{B_1} z_{RL} + z_{RL} v \\ &= -\mathbf{x}^T[\mathbf{C}^T\mathbf{Q}\mathbf{C} + \mathbf{P}\mathbf{B}^{ss}\mathbf{R}^{-1}(\mathbf{B}^{ss})^T\mathbf{P}]\mathbf{x} + 2\mathbf{x}^T\mathbf{P}\mathbf{B_1} z_{RL} + z_{RL} v \\ &< 2\mathbf{x}^T\mathbf{P}\mathbf{B_1} z_{RL} + z_{RL} v.\end{aligned} \tag{34}$$

Choosing

$$v = -k\, z_{RL} - 2\mathbf{x}^T\mathbf{P}\mathbf{B_1}, \quad k > 0, \tag{35}$$

and hence

$$T_{RL} = f_{RLx} r - I_w(\mathbf{K_1}[f_1 \ f_2 \ f_3 \ f_4]^T + k\, z_{RL} + 2\mathbf{x}^T\mathbf{P}\mathbf{B_1}), \tag{36}$$

results in an asymptotically stable origin $\mathbf{x}=\mathbf{0}$, $z_{RL}=0$ of the system (32).

Given T_{RL} from (36) one can calculate the corresponding rear differential drive torque T_R and rear-left wheel torque T_{RL} from Eqs. (16).

A schematic of the proposed control architecture is shown in Fig. 10.

Remark 1. In the calculation of the steady-state cornering conditions exact knowledge of the tire/road friction forces via Pacejka's Magic Formula is assumed. In reality, such information is rarely accurately available due to the number of parameters that affect the tire–road interaction forces. In Velenis et al. (2010) a sensitivity study of the performance of a linear controller stabilizing drifting equilibria of a single-track model in the presence of tire friction uncertainty was discussed. It was shown that the linear quadratic regulator successfully stabilizes the vehicle, with the uncertainty resulting in steady-state errors. Actual implementation of the drifting conditions and the stabilizing control scheme will require real time tire friction estimation as demonstrated, for instance, in Hsu and Gerdes (2005) and Piyabongkarn, Rajamani, Grogg, and Lew (2009). In addition, among the signals required for feedback, the four wheel speeds and the vehicle yaw rate are readily available in modern cars equipped with stability control. The remaining signals may be obtained using state estimation. In Piyabongkarn et al. (2009), for instance, a sideslip angle estimator was designed and experimentally validated, and a low cost GPS was proposed to obtain an accurate measurement of the vehicle speed.

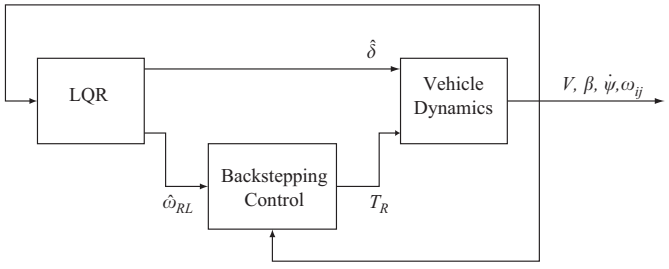

Fig. 10. Control architecture for the stabilization of steady-state cornering conditions.

Remark 2. The control architecture described above stabilizes the vehicle with respect to cornering equilibria across the full range of operation of the tires, including operation on and beyond the tire's adhesion limit. Hence, the controller achieves stability in operating conditions outside the limits enforced by current stability control systems, such as the ESC. In particular, the ESC uses the driver's steering input, the vehicle's yaw rate and/or lateral acceleration to determine the desired path radius using steady-state conditions of a linear bicycle model (Rajamani, 2006). In fact, the ESC aims at restricting the vehicle response within the linear region of operation. It is envisioned that the approach described in this paper will contribute towards new active safety systems, which will employ expert driving skills and techniques and allow the driver to safely exploit the full handling performance of the vehicle during an emergency. Considering a steer-, brake-, drive-by-wire vehicle, the driver's steering command may be used to determine the desired cornering radius similar to the ESC, and the driver's throttle/brake command to determine the desired vehicle velocity. The driver issued cornering radius and velocity would correspond to the target pair (R^{ss}, V^{ss}), and the remaining target equilibrium state and control variables required in the control law (27), (28) and (36) can be determined following the calculations in Section 4. The target condition may lie outside the linear region enforced by the ESC. As long as the target condition is within the physical limits of the vehicle (Fig. 8) the controller will stabilize the target equilibrium. Otherwise the nearest feasible cornering condition will be selected. In this way the driver will be alleviated from the non-intuitive tasks of counter-steering and applying throttle command to control the lateral dynamics of the vehicle, which require expert skills. In addition, the control architecture presented above can be incorporated in an autonomous path following scheme. In Thommyppillai, Evangelou, and Sharp (2009a, 2009b), Sharp, Thommyppillai, and Evangelou (2010), for instance, the optimal gains of a path following controller are calculated using discrete linear quadratic regulator theory with preview, assuming that the vehicle operates near a trim (steady-state) condition. Optimal gains are calculated for a range of trim conditions, leading to an adaptive scheme, where the path following gains change according to the operating condition of the vehicle. In fact, a single transient cornering manoeuvre may involve more than a single equilibrium condition and the controller gains are refreshed accordingly online. The scheme of the references above may be expanded to incorporate limit driving conditions used by expert drivers, as presented in this work.

In the following section the control architecture is implemented to stabilize the vehicle with respect to drifting equilibria similar to those described in Section 2.

6. Simulation results

The results of the implementation of the control scheme of Section 5 using CarSim (2009), a high fidelity vehicle dynamics simulation environment, are presented in the following. The parameters of the vehicle and tire friction model used in the numerical calculations are summarized in Table 1. In addition, the pitch moment of inertia is $I_y = 1401\ \mathrm{kg\,m^2}$, and the roll moment of inertia is $I_x = 198.6\ \mathrm{kg\,m^2}$, while realistic characteristics of stiffness and damping coefficients of each independent suspension are provided by CarSim. For consistency, the tire

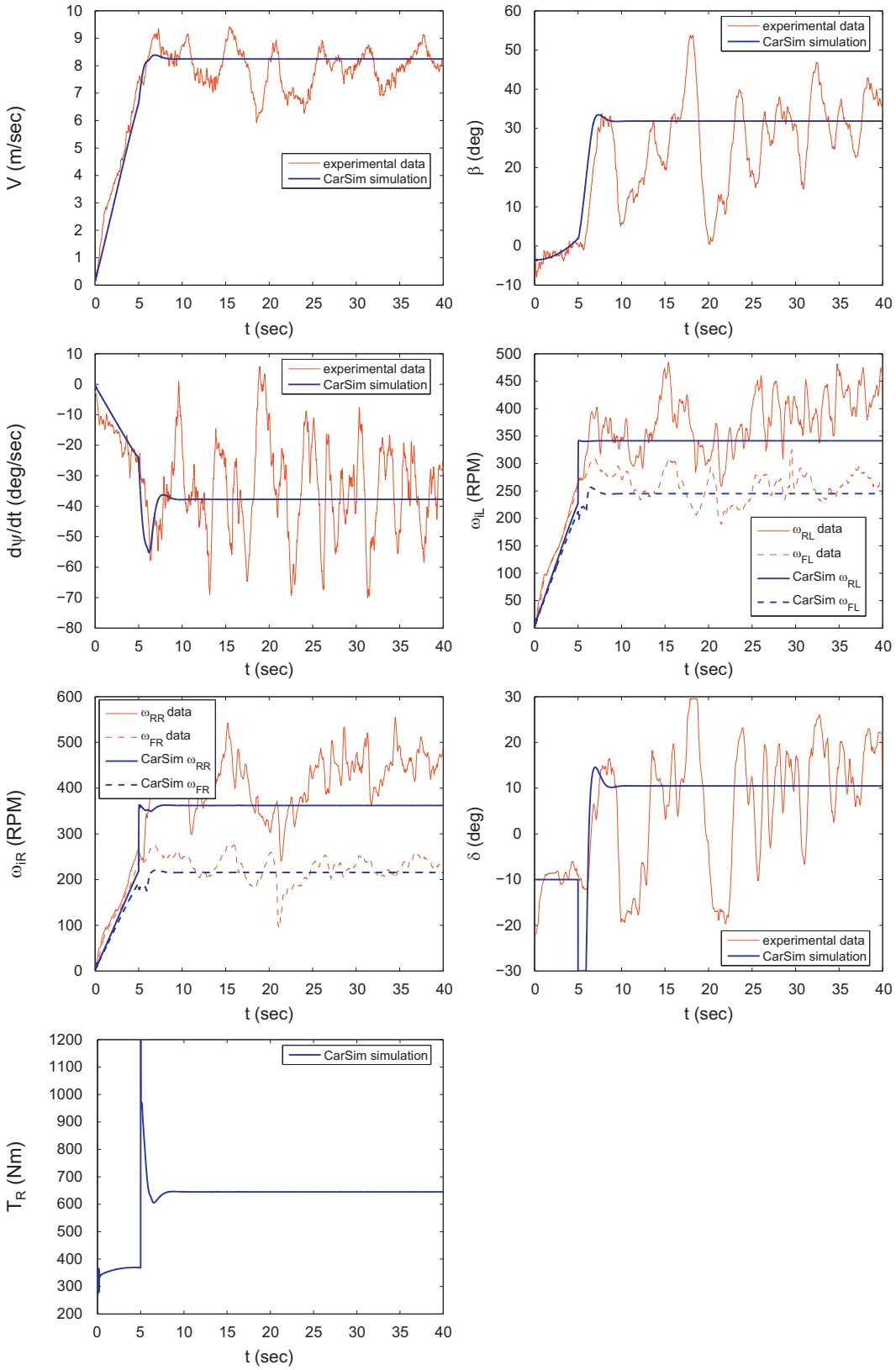

Fig. 11. Vehicle states and control inputs during stabilization with respect to the $R^{ss} = 13$ m cornering equilibrium.

friction model of Section 3 is incorporated in the CarSim simulation. The stabilization of the full-car vehicle model with respect to two steady-state equilibria ($R^{ss} = 13$ and 2 m) as in Table 2 is considered. In both cases the vehicle is initially at a standstill. An open-loop control resembling the driver commands data recorded during the experiment is applied to initiate the maneuver until the vehicle reaches a velocity sufficiently close to the target steady-state value. The control scheme of Section 5 is then engaged to stabilize the vehicle with respect to the prescribed steady-state condition of Table 2.

In the case of $R^{ss} = 13$ m a constant steering command $\delta = -10^{\circ}$ and a constant rear-left wheel torque $T_{RR} = 160$ Nm (and also $T_{RL} = T_{RR} - \Delta T(\Delta\omega)$) are applied during the interval $0 \le t \le 5$ s. For $t > 5$ s the closed-loop control scheme is activated. The vehicle states and control inputs during the stabilization of the vehicle with respect to the $R^{ss} = 13$ m equilibrium are shown in Fig. 11. In order

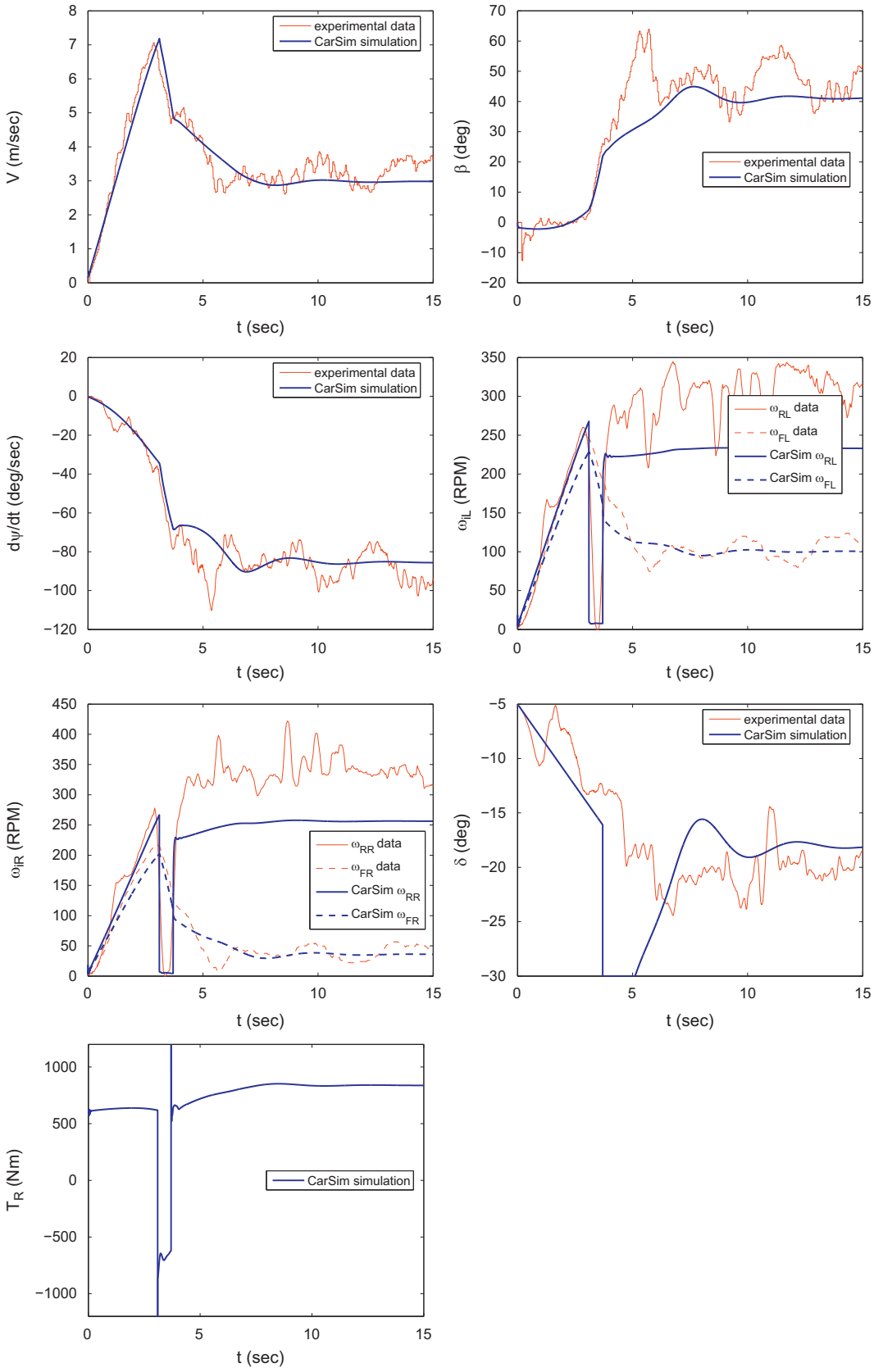

Fig. 12. Vehicle states and control inputs during stabilization with respect to the $R^{ss} = 2$ m cornering equilibrium.

to avoid unrealistic control inputs, saturation of the magnitude of the steering angle at 30° has been imposed. The saturation limit was instantaneously reached at the instant of switching from the open-loop to the closed-loop control ($t=5$ s). For comparison, the response data of the test vehicle during the data collection experiment are superimposed. In the absence of disturbances, the CarSim model reaches the steady-state condition within 10 s and then maintains constant states and control inputs, as opposed to the oscillatory behavior of the vehicle experimental data. Once again, the human driver data variations near the steady-state condition are thought to emerge from physical disturbances compensated by the human controller. Response delays, sensory thresholds and response inaccuracy of the human driver may also contribute to discrepancies with respect to the backstepping controller performance. Fig. 13 shows the trajectory of the vehicle during stabilization, generated by the animation tool of CarSim.

In the case of $R^{ss}=2$ m, a constant steering command $\delta=-15^{\circ}$ during the interval $0\le t\le 3.5$ s is applied. During the interval $0\le t\le 3.1$ s a constant accelerating torque $T_{RR}=300$ Nm (and also $T_{RL}=T_{RR}-\Delta T(\Delta\omega)$) is used, followed by a braking command $T_{RL}=-500\,\omega_{RL}$, $T_{RR}=-500\,\omega_{RR}$ (with T_{Rj} in Nm and ω_{Rj} in rad/s) until $t=3.5$ s, emulating the handbrake command recorded in the experiment. For $t>3.5$ s the closed-loop control scheme is engaged. The vehicle states and control inputs during the stabilization of the vehicle with respect to the $R^{ss}=2$ m equilibrium are shown in Fig. 12, where the response data of the test vehicle during the data collection experiment are superimposed for comparison. One can observe the close resemblance in the response of the simulation model to the experimental data of the test vehicle response. Fig. 14 shows the trajectory of the vehicle during stabilization, generated by the animation tool of CarSim.

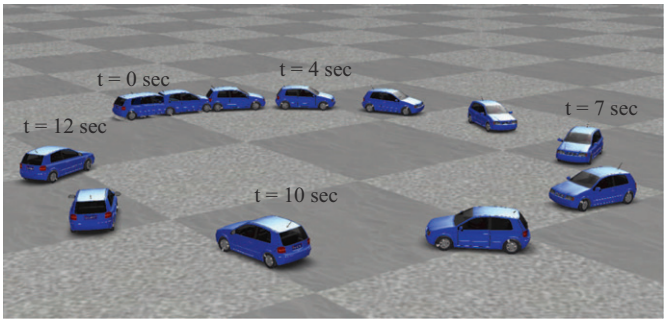

Fig. 13. Vehicle trajectory during stabilization with respect to the $R^{ss}=13$ m cornering equilibrium.

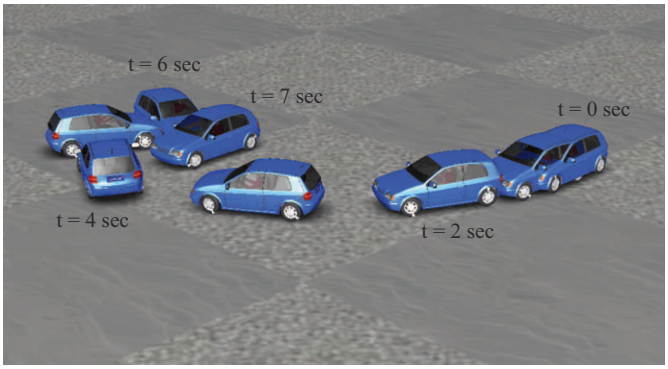

Fig. 14. Vehicle trajectory during stabilization with respect to the $R^{ss}=2$ m cornering equilibrium.

7. Conclusions

The stabilization of RWD vehicles with respect to cornering equilibria characterized by aggressive sideslip angles was studied in this work. The results of a data collection experiment during execution of steady-state drifting by an expert driver were analyzed, concluding that RWD vehicle drifting stabilization requires a combination of throttle and steering regulation. The data also revealed that drifting equilibria exist at path radii considerably smaller than the kinematic turning radius of the vehicle, expanding its mobility capabilities. Steady-state drifting states and inputs, which closely match the experimental data, can be computed numerically using a full-car vehicle model with nonlinear tire characteristics and realistic drive-train modelling, as demonstrated in this paper. In addition, a backstepping control scheme can be used to stabilize the vehicle with respect to drifting cornering equilibria. The controller designed in this work uses combined steering angle and drive torque inputs, correlating directly to the human driver commands. The controller was successfully validated via implementation in a high-fidelity simulation environment. The simulation scenarios emulated the cornering conditions recorded during the experiment, including cornering along an extremely small path radius.

Acknowledgments

The work of E. Velenis was supported by a Marie Curie International Reintegration Grant within the 7th European Community Framework Programme, and a Brunel University BRIEF award. The work of D. Katzourakis and R. Happee was supported by the Automotive Development Centre of SKF as part of the project Mobility Intelligence using Load based Lateral Stability (MILLS). The work of E. Frazzoli was supported by ARO award W911NF-07-1-0499. The work of P. Tsiotras was supported by ARO award no. W911NF-05-1-0331 and NSF GOALI award no. CMMI-0727768. The authors would like to thank three anonymous reviewers of this paper for their constructive suggestions.

References

Abdulrahim, M. (2006). On the dynamics of automobile drifting. In *SAE world congress*, Detroit, MI, April 3–6.

Bakker, E., Nyborg, L., & Pacejka, H. (1987). Tyre modelling for use in vehicle dynamics studies. SAE Paper No. 870421.

CarSim (2009). CarSim User Manual. Mechanical Simulation Corp., Ann Arbor, MI.

Edelmann, J., & Plöchl, M. (2009). Handling characteristics and stability of the steady-state powerslide motion of an automobile. *Regular and Chaotic Dynamics*, *14*(6), 682–692.

Frazzoli, E. (2008). Discussion on "optimality properties and driver input parameterization for trail-braking cornering". *European Journal of Control*, *14*(4).

Gillespie, T. (1992). Fundamentals of vehicle dynamics. Society of Automotive Engineers SAE International, Warrendale, PA, USA.

Hindiyeh, R., & Gerdes, J. (2009). Equilibrium analysis of drifting vehicles for control design. In *Proceedings of the ASME 2009 dynamic systems and control conference*, Hollywood, CA, USA, October 12–14.

Hsu, Y., & Gerdes, J. (2005). Stabilization of a steer-by-wire vehicle at the limits of handling using feedback linearization. In *ASME international mechanical engineering congress and exposition*, Orlando, FL, USA, November 5–11.

Katzourakis, D., Velenis, E., Abbink, D., Happee, R., & Holweg, E. Race car instrumentation for driving behaviour studies. *IEEE Transactions on Instrumentation and Measurement*, doi:10.1109/TIM.2011.2164281.

Kokotovic, P. (1992). The joy of feedback: Monolinear and adaptive. *IEEE Control Systems Magazine*, *12*(3), 7–17.

Ono, E., Hosoe, S., Tuan, H., & Doi, S. (1998). Bifurcation in vehicle dynamics and robust front wheel steering control. *IEEE Transactions on Control Systems Technology*, *6*(3), 412–420.

Piyabongkarn, D., Rajamani, R., Grogg, J., & Lew, J. (2009). Development and experimental evaluation of a slip angle estimator for vehicle stability control. *IEEE Transactions on Control Systems Technology*, *17*(1), 78–88.

Rajamani, R. (2006). *Vehicle dynamics and control*. New York: Springer Science and Business Media.

Sharp, R., Thommyppillai, M., & Evangelou, S. (2010). Towards a model of a high-performance driver for circuit-racing cars. In *10th international symposium on advanced vehicle control*, Loughborough, UK, August 22–26.

Thommyppillai, M., Evangelou, S., & Sharp, R. (2009a). Advances in the development of a virtual car driver. *Multibody System Dynamics*, *22*(3), 245–267.

Thommyppillai, M., Evangelou, S., & Sharp, R. (2009b). Car driving at the limit by adaptive linear optimal preview control. *Vehicle System Dynamics*, *47*(12), 1535–1550.

van Zanten, A. T., Erhardt, R., Landesfeind, K., & Pfaff, G. (2000). Vehicle stabilization by the vehicle dynamics control system ESP. In *IFAC mechatronic systems* (pp. 95–102), Darmstadt, Germany.

Velenis, E., Frazzoli, E., & Tsiotras, P. (2009). On steady-state cornering equilibria for wheeled vehicles with drift. In *48th IEEE conference on decision and control*, Shanghai, China, December 16–18.

Velenis, E., Frazzoli, E., & Tsiotras, P. (2010). Steady-state cornering equilibria and stabilization for a vehicle during extreme operating conditions. *International Journal of Vehicle Autonomous Systems, Special Issue on Autonomous and Semi-Autonomous Control for Safe Driving of Ground Vehicles*, *8*(2/3), 217–241.

Velenis, E., & Tsiotras, P. (2005). Minimum time vs maximum exit velocity path optimization during cornering. In *2005 IEEE international symposium on industrial electronics* (pp. 355–360), Dubrovnic, Croatia, June.

Velenis, E., Tsiotras, P., & Lu, J. (2007a). Modeling aggressive maneuvers on loose surfaces: Data analysis and input parameterization. In *Proceedings of the 2007 mediterranean conference on control and automation*, Athens, Greece, June 27–29.

Velenis, E., Tsiotras, P., & Lu, J. (2007b). Modeling aggressive maneuvers on loose surfaces: The cases of trail-braking and pendulum-turn. In *Proceedings of the 2007 European control conference*, Kos, Greece, July 2–5.

Velenis, E., Tsiotras, P., & Lu, J. (2008). Optimality properties and driver input parameterization for trail-braking cornering. *European Journal of Control*, *14*(4), 308–320.

Voser, C., Hindiyeh, R., & Gerdes, J. (2009). Analysis and control of high sideslip maneuvers. In *21st international symposium on dynamics of vehicles on roads and tracks*, Stockholm, Sweden, August 17–21.